Paper # 070IC-0355 **Topic: Internal combustion and gas turbine engines** SAND2013-2181C

8th U. S. National Combustion Meeting
Organized by the Western States Section of the Combustion Institute
and hosted by the University of Utah
May 19-22, 2013

Extinction-based Imaging of Soot Processes over a Range of Diesel Operating Conditions

Scott A. Skeen[1] *Julien Manin*[1] *Kristine Dalen*[2] *Lyle M. Pickett*[1]

[1]*Combustion Research Facility, Sandia National Lab, 7011 East Ave. Livermore, CA 94551*
[2]*Department of Mechanical Engineering, Technical University of Denmark, 2800 Kgs. Lyngby*

In this work, we applied a suite of optical diagnostics to measure the soot volume fraction, ignition delay time, and lift-off length of n-dodecane spray flames burning in a constant-volume, high-pressure, high-temperature vessel—while systematically varying ambient temperature, density, and oxygen concentration. The fuel was injected with a common-rail diesel injector equipped with a single 90-μm diameter orifice belonging to the family of injectors used in the Engine Combustion Network (ECN). The 2-D temporal evolution of the soot volume fraction was measured using a high-speed two-color diffused back illumination technique. For validation of the two-color technique and comparison with prior work, we also simultaneously measured the optical thickness, *KL*, using laser extinction. Ignition delay times and the temporal evolution of the lift-off length were measured using a second high-speed imaging setup, and we measured the quasi-steady lift-off length using an intensified camera filtered to detect OH chemiluminescence. As in previous works, we used the flame lift-off lengths to aid our analyses of the soot measurements. Consistent with previous studies using LII in conjunction with laser-extinction to measure f_v, the peak soot level in a fuel jet increases with increasing ambient gas temperature. Higher ambient temperatures also promote soot oxidation at the flame tip. Higher ambient densities enhance soot formation, even after accounting for the increase in number density with pressure. Experiments performed while varying both temperature and ambient oxygen concentration reveal important results with respect to the use of exhaust gas recirculation (EGR). Strategies promoting high ambient temperatures with high-EGR (reduced O_2 concentration) should be avoided as soot formation is enhanced by the higher ambient temperature while soot oxidation is hindered by the lack of oxidizing species. Strategies using high-EGR with low-ambient temperatures show promise for substantial reductions in in-cylinder soot. The two-color diagnostic shows promise for identifying spatial variations in soot physical properties, mainly due to apparent changes in the local soot refractive index.

1. Introduction

Although direct-injection (DI) diesel engines have the capacity for significantly higher efficiencies than spark-ignited gasoline engines, they can be plagued by particulate matter (PM) emissions (mainly soot) formed in the fuel-rich regions of the combusting fuel jets. More stringent PM emissions standards for diesel engines have led to the use of additional exhaust after-treatment such as diesel particulate filters, which increase the cost of diesel engine production while negatively impacting fuel economy. A more economical approach to reducing soot emissions from DI diesel engines lies in the development of combustion strategies to reduce or eliminate soot in-cylinder. The successful development of such strategies, by experimental or computational means, can benefit from time-resolved, quantified measurements of soot volume fraction (f_v) as a function of the available operational parameters.

Laser extinction (LE) and laser-induced incandescence (LII) represent the most commonly used in-situ optical diagnostics used to measure f_v in flames. In some cases, laser scattering measurements have been coupled to LE measurements to obtain additional information about primary particles and aggregates (Puri et al. 1993). While single-color LE measurements alone can only provide information about f_v, LII measurements in conjunction with an accurate physical model can yield information about f_v and primary particle size. In both cases, knowledge of the particles' optical properties (i.e., refractive index) is required. The uncertainty in the refractive index of soot is well-documented and is generally accepted to be large (Sorensen 2001). The vast majority of LE and LII measurements have been made at atmospheric pressure and under steady, laminar flame conditions.

Prior studies by our group have used 2-D planar LII in conjunction with path-averaged LE to obtain quantitative f_v measurements during the quasi-steady period of spray combustion at pressures and temperatures relevant to diesel engines (Pickett and Siebers 2004). Because the duration of the injection and combustion event for these studies is less than 10 milliseconds, the 10 Hz Nd:YAG lasers commonly used for LII provide only a single image per injection, but no information about the temporal evolution of soot during a single injection event. This drawback may be avoided by using high-power burst lasers for high repetition-rate LII (Sjöholm et al. 2011); however, this technology is still under development and we anticipate that cost will prohibit the widespread use of such systems in the near-term. Another weakness of 2-D planar LII is exposed when soot concentrations are high enough to cause significant laser attenuation. As an example, for an optical thickness (KL) of 1, less than 40% of the original laser energy is transmitted to soot particles later in the laser path. At KL = 2, almost 90% of the laser energy has been absorbed. In atmospheric pressure flames, laser fluences (laser energy per unit area) greater than ~ 0.2 J/cm^2 (for 532 nm light) heat soot particles to their sublimation temperature and the LII signal is relatively insensitive to laser fluence variations (Schulz et al. 2006). For this reason, LII experiments seeking quantitative measurements of soot volume fraction typically operate in this so-called "plateau" regime (Schulz, Kock et al. 2006). As flames become optically thick, however, LII signal from particles found later in the laser path can be significantly reduced. Further, dense soot clouds outside the laser sheet can block incandescence signal from reaching the detector—a phenomenon referred to as signal trapping. Compensating for these effects can be difficult and in general yield a negative impact on soot level quantification (Pickett and Siebers 2006). To investigate the temporal evolution of f_v in high-pressure, high-temperature spray flames while avoiding the aforementioned complexities of LII, we have developed a high-speed 2-D back illumination extinction technique.

In this work, we measured the 2-D temporal evolution of f_v in high-pressure spray flames using a newly-developed high-speed two-color diffused back illumination extinction technique. The new diagnostic was validated by simultaneously measuring the path-averaged optical thickness, KL, using laser extinction. To monitor several critical factors impacting soot, we measured ignition delay times using a second high-speed imaging setup and the quasi-steady lift-off length (H) using an intensified camera filtered to detect OH chemiluminescence.

In addition to providing quantitative measurements to aid in the development of predictive models, a key purpose of the Engine Combustion Network (ECN, see www.sandia.gov/ECN) involves facilitating and promoting comparisons of experimental data acquired under nearly identical operating conditions, but at different institutions using a variety of high-pressure, high-temperature facilities. Presently, quasi-steady lift-off length measurements for the "Spray A" target condition and its parametric variations have been performed by a number of institutions. Beyond effects attributable to the different facilities, the specific injector (although nominally identical (Kastengren et al. 2013)) used in each institution or experiment, may have a significant impact on the results. The lift-off length measurements in this work are compared to previous measurements realized in the same facility at Sandia National Laboratories, but with a different injector. The two injectors have the same nominal specifications from the manufacturer; thus, these measurements provide some indication of the effects of manufacturing tolerances on spray development and mixing, looking specifically at the lift-off length.

2. Methods

Combustion Vessel

Sprays of n-dodecane ($C_{12}H_{26}$) were injected into a high pressure (up to 35 MPa), high temperature (up to 1400 K) constant-volume combustion vessel**Error! Reference source not found.**. The targeted operating conditions of this study are typical of those encountered inside the combustion chamber of modern diesel engines. A full description of the combustion vessel and its operation can be found in (Siebers 1998). Briefly, the vessel is nearly cubical with a volume of approximately 1 L. Sapphire windows provide optical access to the spray event from four sides. Prior to and during operation, the temperature of the entire vessel is maintained at 188 ºC by electric heaters. Spark-ignition of a combustible gas mixture rapidly elevates the pressure and temperature within the vessel. The spray event (i.e., fuel injection) takes place when the desired thermodynamic conditions are achieved after a short cool-down period. These experiments used a common-rail diesel fuel injector equipped with a single 90-µm diameter orifice (# 370) belonging to the family of "Spray A" ECN injectors. The injection pressure was 1500 bar. In addition to the target condition (Spray A), we performed a parametric study by changing ambient temperature, ambient oxygen concentration, and discharge density to evaluate their effects on soot formation. The nominal ambient experimental conditions of this study are provided in Table 1.

Table 1. Nominal ambient experimental conditions

Temperature [K]	750	800	850	900	1000	1100	1200
O_2 [vol%]	15	15	15	13/15/21	13/15/21	13/15/21	13/15/21
Density [kg/m^3]	22.8	22.8	22.8	7.6/15.2/22.8	7.6/15.2/22.8	7.6/15.2/22.8	7.6/15.2/22.8

OH Chemiluminescence Imaging and Lift-off Length

We measured the quasi-steady lift-off length as described in (Higgins and Siebers 2001; Siebers and Higgins 2001). An intensified CCD camera (Princeton Instruments, PI-Max 3) equipped with a 308 nm (10 nm FWHM) bandpass filter collected excited state OH (OH*) chemiluminescence from the burning fuel jet. The short-lived OH chemiluminescence emission dominates in the lift-off length region as it results from the high-heat-release reactions occurring under near-stoichiometric conditions, which are representative of the lifted diffusion flame. Image acquisition began after autoignition occurred and after the transient jet tip had passed through the field of view. We stopped image acquisition prior to the end of injection, resulting in a time-averaged image free from the appearance of turbulent fluctuations.

In accordance with previous results, OH chemiluminescence appears at a well-defined distance from the injector orifice. The signal is characterized initially by a steep gradient followed by a plateau region (Pickett and Siebers 2004). For Spray A, we define the lift-off length as the axial distance between the orifice and the location where OH chemiluminescence intensity is 50% of the maximum prior to the plateau region. We then use the 50% threshold from Spray A as the OH chemiluminescence intensity threshold when evaluating sprays combusting under different ambient temperature, density, and oxygen concentration conditions.

Luminosity Imaging and Ignition Delay Time

In addition to quasi-steady lift-off lengths, we measured ignition delay times using a high-speed camera at 20000 frames per second (fps) equipped with a 600-nm short-pass filter to suppress the high intensity soot luminosity and take advantage of the camera's dynamic range. As with the lift-off length measurements, we compare the ignition delay times measured here with those measured previously to confirm that the target ambient conditions were achieved.

2-D High-Speed Extinction

The main components of the 2-D high-speed extinction setup consists of high-output, ultra-fast, blue (406 nm) and green (519 nm) LEDs, a dichroic beam splitter, engineered diffusers, a field lens, and a high-speed camera (running at 82 kfps) equipped with the appropriate band-pass filters as shown in Figure 1. The diffusers have a 50^o circular pattern and the field lens is a Fresnel type with a focal length of 152 mm. The engineered diffusers in conjunction with the Fresnel lens create a large (60 mm diameter) uniformly illuminated background with minimal light intensity losses (more than 90% transmission) (Ghandhi and Heim 2009). This light source setup directs a bundle of diffused rays toward the object plane resulting in minimal light extinction by density gradients (i.e., beam steering, schlieren effects).

The background corrected 2-D extinction measurements were converted to optical thickness, *KL*, using the well-known Beer-Lambert law.

$$I/I_0 = \exp(-KL) \quad (1)$$

In Eq. 1, I is the transmitted LED intensity, I_0 is the incident intensity, K is the dimensional extinction coefficient, and L is the path length through the soot cloud. We corrected the transmitted intensity for flame luminosity by capturing a frame between the blue and green LED pulses when only flame luminosity was present (i.e. with both LEDs turned off). For the highest ambient temperature cases (1100 and 1200 K), we observed infrequent, intermittent localized regions where flame luminosity was larger than the sum of the transmitted LED intensity and the flame luminosity in the surrounding frames. This phenomenon was attributed to the rapid spatial fluctuations in extinction and flame emission. Specifically, local regions of high extinction and high flame emission observed during the LED pulse move both downstream and stochastically during the time between two captured frames. Spatial mismatches between a region of high extinction and high flame emission can thus result in negative values for the background corrected transmitted intensity, I. We minimized these effects via a weighted temporal averaging scheme. Nevertheless, our analysis required the specification of an upper threshold limit for *KL*. We assessed the uncertainty associated with this phenomenon in the higher ambient temperature cases as ±10%, which, for example, is well below the uncertainty due to variation in soot refractive index.

We derived soot volume fraction, f_v, from the *KL* images using the following relationships based on small particle Mie theory.

$$f_v = K\lambda/k_e \quad (2)$$

$$k_e = (1+\alpha_{sa})6\pi E(m) \quad (3)$$

In Eq. 2 and 3, λ is the wavelength of incident light, k_e is the non-dimensional extinction coefficient, α_{sa} is the scattering-to-absorption ratio, and $E(m)$ is the imaginary part of $(m^2-1)/(m^2+2)$, in which m is the complex refractive index of soot.

We calculated the non-dimensional extinction coefficient (k_e) using Rayleigh-Debye-Gans (RDG) theory for fractal aggregates following the work of Ko□ylu□ and Faeth (Koylu and Faeth 1994; Koylu and Faeth 1994). In our analysis, we specified the number of primary particles per aggregate (N_p) as 150, with a primary particle diameter (d_p) of 16 nm (Aizawa et al. 2012; Kook and Pickett 2012). The fractal dimension, D_f, associated with the above parameters is 1.79. As noted by Shaddix et al. (Shaddix et al. 2005), the RDG scattering approximation is considered to be accurate provided that $D_f < 2$. For simplicity, the refractive index was held constant at m = 1.75-1.03i (Williams et al. 2007) for the two wavelengths evaluated resulting in k_e values of 7.46 and 7.76 for the green and blue light, respectively. The refractive index reported by Williams et al. (Williams, Shaddix et al. 2007) is considered more appropriate for the present work because they derived m by measuring the k_e of soot particles within the flame, as opposed to prior studies that measured the k_e of post-flame soot. We understand that the refractive index of soot depends on the soot morphology, primary particle size and structure, and the wavelength of incident light. A full analysis on the effects of assumed d_p, N_p and m on our evaluation of f_v, as well as the uncertainty associated with the use of RDG theory for large m and when multiple internal scattering may be important, is beyond the scope of this work and will be addressed in a follow-on paper.

At the pressures and temperatures of this study, extinction due to beam steering effects could not be completely avoided. Because our diffused light source is not perfectly Lambertian, beam steering can increase local transmission if diffused ray bundles are preferentially steered toward a common image point. At locations where light is steered away from the expected path, extinction occurs. Upon time averaging, the measured extinction under non-sooting flame conditions was near zero. In the individual time-resolved images, however, extinction caused by beam steering defined our lower *KL* detection limit. For non-sooting cases, this lower limit was determined to be approximately 0.1. For path lengths on the order of 10 mm and a non-dimensional extinction coefficient (k_e) near 8, this corresponds to a lower detection limit of about 1 ppm for f_v. Based on the factors considered above, we assign a conservative uncertainty of ± 15% to the quantitative soot volume fractions presented below.

For validation of the 2-D technique, laser-extinction measurements were made using a 10-mW, 1-mm HeNe (632.8 nm) laser gated at 100 kHz by an acousto-optic modulator. The full details of this setup are available in (Pickett and Siebers 2004). The HeNe laser passed through the flame axis 60 mm downstream of the injector orifice. Collection optics and components for the laser extinction measurement included a 50-mm diameter, 200-mm focal length lens to collect the laser after passing through the testing section, a 100-mm integrating sphere, a 633 nm (1 nm FWHM) bandpass filter sandwiched between a 75-mm focal length lens pair, and a photodiode. Previous work has demonstrated this system's insensitivity to extinction caused by beam-steering (Pickett and Siebers 2004).

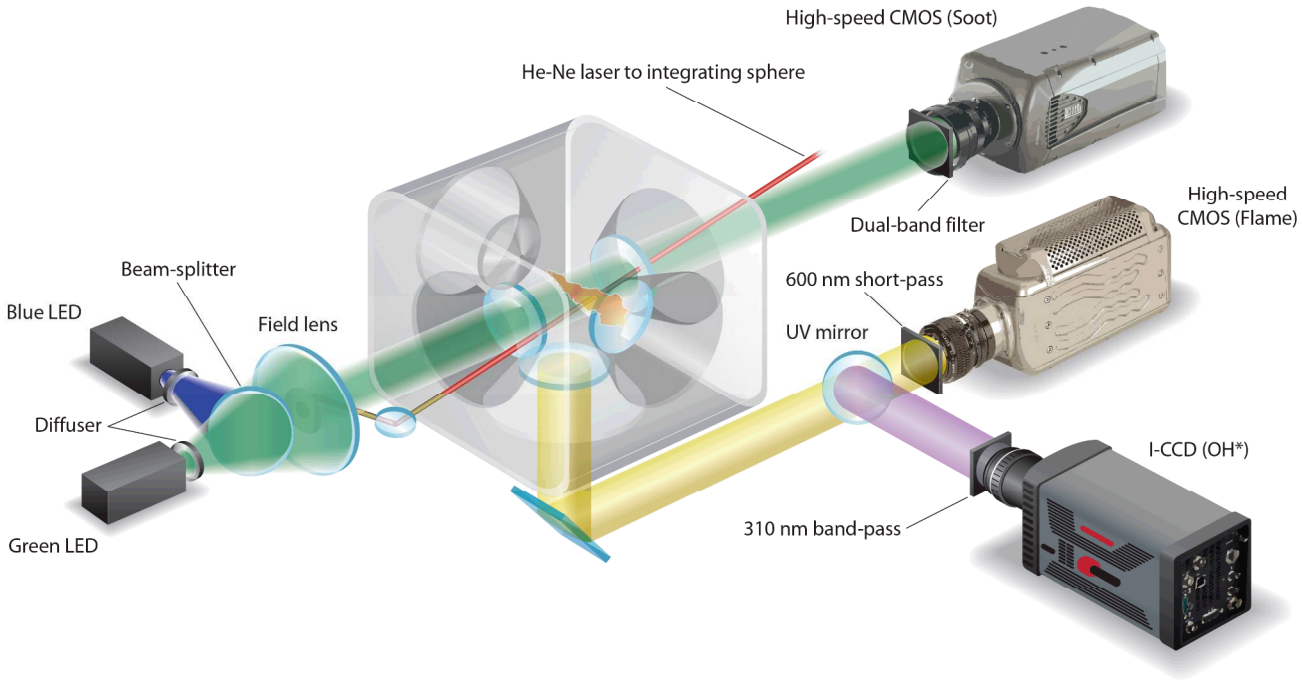

Figure 1. Schematic of experimental setup

3. Results and Discussion

3.1 Lift-off Length and Ignition Delay Time

Lift-off length as a function of the vessel's core temperature during injection is shown in Figure 2. The current data obtained using Injector 370 are distinguished from those acquired previously with Injector 677. The figure also includes lift-off lengths as a function of core temperature at different ambient densities and oxygen concentrations.

The close agreement of the current and previous results at a density of 22.8 kg/m3 and O_2 concentration of 15% suggests that differences in Injectors 370 and 677 due to manufacturing tolerances are not discernible in measured spray flame lift-off lengths. In agreement with previous findings, the data in Figure 2 shows that lift-off length is inversely related to ambient density and oxygen concentration. That is, lower ambient densities and lower oxygen concentrations lead to longer lift-off lengths. Higgins and Siebers (Higgins and Siebers 2001) and Siebers and Higgins (Siebers and Higgins 2001) provide a detailed analysis discussing the effects of ambient temperature, density, and oxygen concentration on lift-off length.

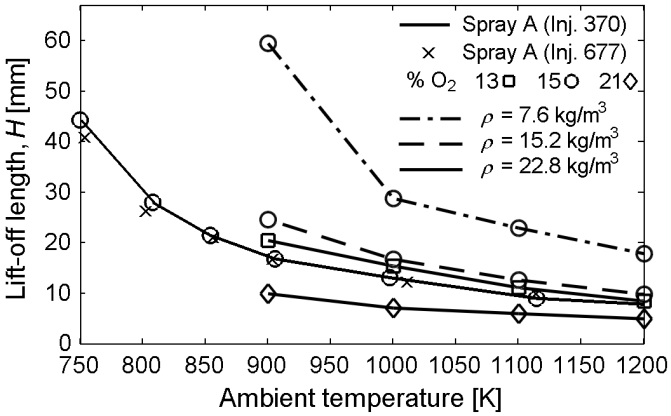

Figure 2. Lift-off length as a function of ambient temperature. Ambient densities are distinguished by the line style. Ambient oxygen concentrations are distinguished by the symbols. Data for Spray A with injector 677 were taken from the ECN database (www.sandia.gov/ECN).

Ignition delay times as a function of ambient temperature are shown in Figure 3. The different ambient densities are distinguished by the line style, while the different oxygen concentrations are distinguished by the symbols. Spray A data from the ECN database (www.sandia.gov/ECN) are included. These data correspond to Injector 677. In general, the Spray A data corresponding to Injector 370 agree well with that obtained using Injector 677. Consistent with the lift-off length measurement, the times measured in this work are somewhat longer than those measured previously at ambient temperatures of 750 K and 800 K. As demonstrated in previous work, ignition delay times decrease with increasing ambient density, oxygen concentration, and temperature. Good agreement with

previous results for both lift-off length and ignition delay time confirm that the targeted temperatures, densities, and O_2 concentrations were met in the present study.

3.2 Time-resolved extinction measurements

3.2.1 Optical Thickness and Soot Volume Fraction

Temporally resolved images showing the progression of the soot optical thickness (*KL*) during injection at the Spay A condition are presented in Figure 4. In these images, the fuel injector is located to the left and the flame is propagating from left to right. The *KL* values in this figure correspond to extinction of the blue (406 nm) LED at Spray A conditions. Under these conditions, soot is first detected at an axial location approximately 35 mm from the injector orifice less than 1 millisecond after the start of injection (ASOI). Though *KL* time-sequences are not shown here for the other ambient conditions studied, the axial distance from the injector orifice to the location where soot is first observed and the time to soot ASOI decrease with increasing temperature, density, and oxygen concentration.

The images in Figure 4 show that a large amount of soot forms in the head of the jet as it propagates into the ambient. The soot cloud associated with the head also begins separating from the upstream soot cloud in the region between 50 and 60 mm at about 2 ms ASOI. At 2.75 ms ASOI, the head has completely separated from the upstream soot cloud. This occurs presumably due to rapid entrainment of the ambient oxidizer behind the jet head leading to a brief transient period of enhanced mixing and soot oxidation. Such phenomena were observed here under a wide range of ambient conditions, and may be important in understanding the efficacy of multiple injection strategies (O'Connor and Musculus 2013).

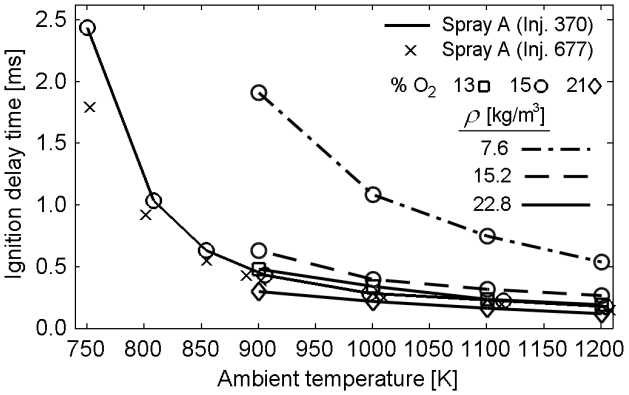

Figure 3. Semi-log plot of ignition delays as a function of ambient temperature. Ambient densities are distinguished by the line style. Ambient oxygen concentrations are distinguished by the symbols. Data for Spray A with injector 677 were taken from the ECN database (www.sandia.gov/ECN).

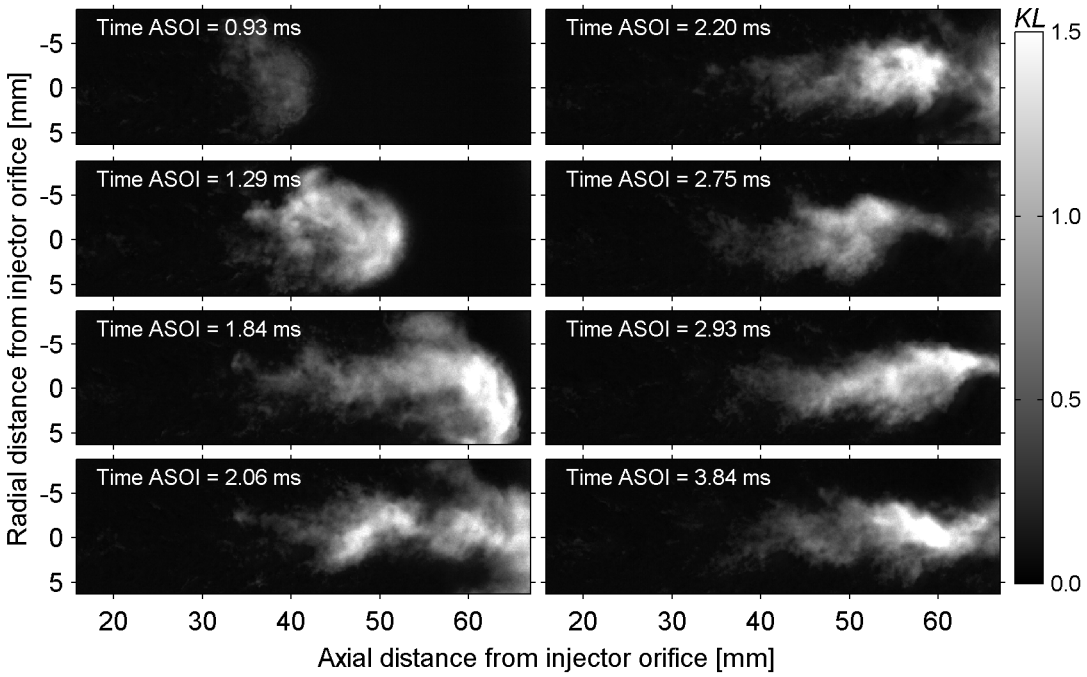

Figure 4. Time-sequenced images of the soot optical thickness (*KL*) at Spray A conditions (i.e., T = 900 K, ρ = 22.8 kg/m^3 and 15% O_2).

The quasi-steady time period of the spray flame begins after the head of the jet passes through the camera's field of view and ends at injector closing. We determined *K* for use in Eq. 2 via tomographic inversion of time- and ensemble-averaged *KL* images from multiple identical injection events. Time-averaging was performed over the quasi-steady period of the flame (approximately 4 ms, representing more than 100 images per injection and per color). Ensemble averaging included a minimum of 5 injections for each specific experimental condition. The averaged *KL* images result in a relatively smooth (i.e., free from stochastic variations) and nearly axisymmetric *KL* field as shown in Figure 5. Note that the results in Figure 5 only correspond to extinction of the blue LED. Results for the green LED will be discussed later. When comparing these five cases, we first observe that the maximum *KL* under the 1200 K ambient condition is more than one order of magnitude larger than that at an ambient temperature of 850 K. As previously mentioned, Figure 5 also shows that soot formation begins closer to the injector orifice for the higher temperature cases.

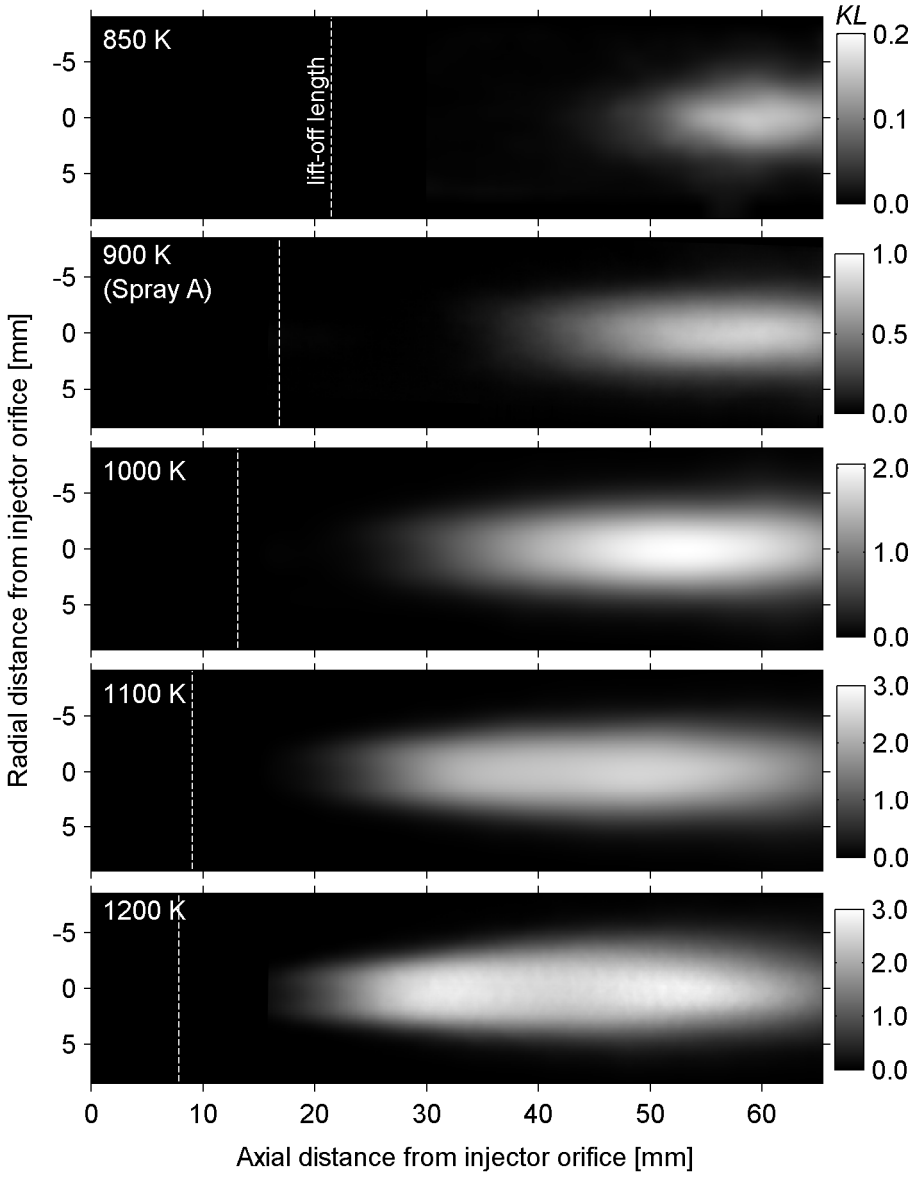

Figure 5. Averaged images of the soot optical thickness (*KL*) for the 850 K – 1200 K ambient temperature sweep at an ambient density of 22.8 kg/m^3 and ambient O_2 concentration of 15% (by volume). The lift-off length is indicated by the dashed line.

We performed the tomographic reconstruction of the *KL* field using an inverse Radon transform, which then returns f_v after Eq. 2 has been applied. Figure 6 shows the 2-D f_v field in the plane corresponding to the center of the flame axis for the 850 K – 1200 K conditions at an ambient density of 22.8 kg/m^3 and ambient O_2 concentration of 15% by volume. The plane cut in the tomographic reconstruction yielding f_v more clearly reveals the higher soot concentrations near the periphery of the 1100 and 1200 K cases at the flame's base. These soot "wings" as they have been called, provide further evidence that spray flames having shorter lift-off lengths have partially-premixed mixtures that are more fuel (Pickett and Siebers 2006). An interesting feature is observed in the 1100 K and 1200 K cases at an axial position between about 35 mm and 50 mm from the injector orifice. Near 35 mm, f_v appears to decrease in the central region of the flame. The phenomenon is more apparent for the 1200 K case. We suspect that this may be due to the intermittent localized regions in the 1100 K and 1200 K cases where the background luminosity was larger than that observed during the extinction image. Future work will entail increasing the LED intensity, increasing the optical density of the neutral density filter to block more flame emission, and reducing the bandwidth of the dual-bandpass filter. Increasing the number of identical injections for ensemble averaging will also provide better resolution and higher fidelity.

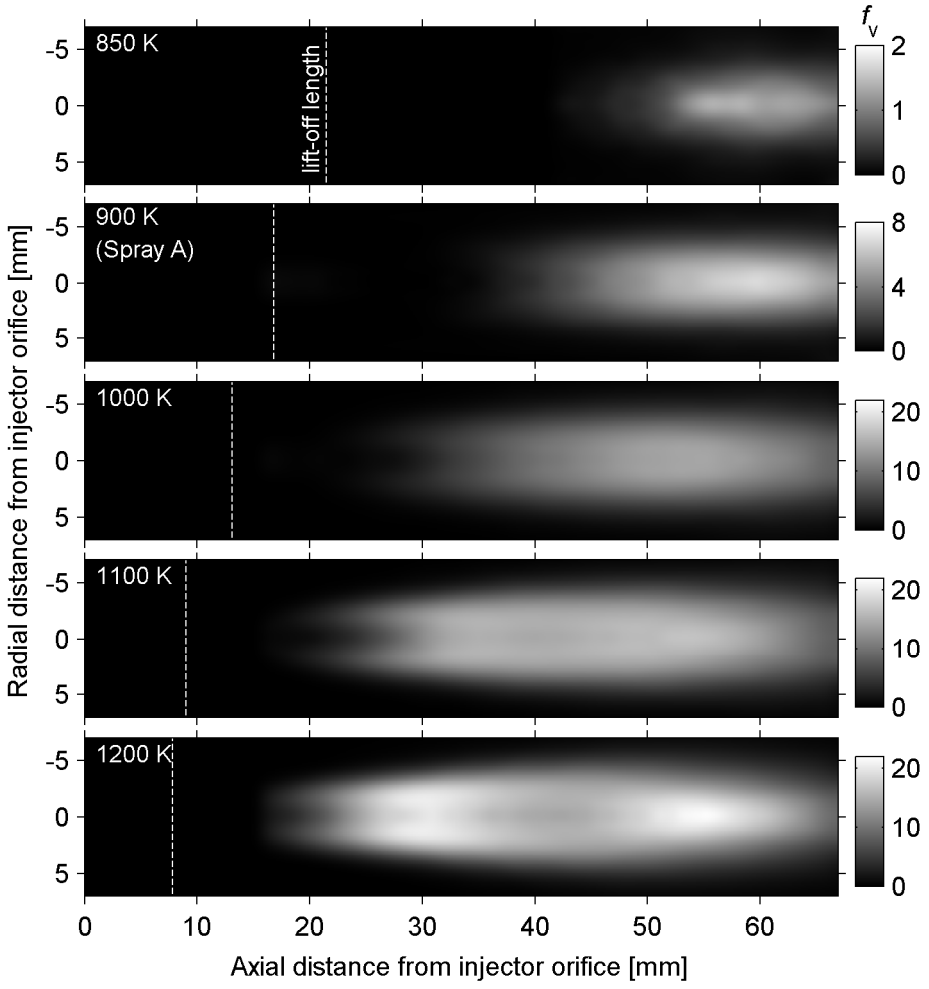

Figure 6. Soot volume fraction (f_v) in the plane corresponding to center of the flame axis for the 850 K – 1200 K ambient temperature sweep at an ambient density of 22.8 kg/m^3 and ambient O_2 concentration of 15% (by volume).

3.2.2 Unique results from two-color extinction

A novel feature of the two-color extinction diagnostic is observed when comparing f_v evaluated with blue and green incident light under a given condition. Figure 7 shows the difference between the soot volume fraction based on our analysis of green light extinction ($f_{v,green}$) and that based on our analysis of the blue light extinction ($f_{v,blue}$). For the 900 K (Spray A) case shown in the upper panel, $f_{v,blue}$ is generally larger than $f_{v,green}$. Assuming that molecular absorption of light near 400 nm is insignificant, then $f_{v,blue}$ and $f_{v,green}$ should be equal. This can be achieved by adjusting the non-dimensional extinction coefficient, k_e, in Eq. 2. Holding m and d_p constant while varying N_p, the RDG scattering approximation yields $k_{e,blue}/k_{e,green}$ ratios that increase slightly with increasing N_p. Thus, the difference between $f_{v,blue}$ and $f_{v,green}$ in the upper panel of Figure 7 might suggest that we should have used a larger value for N_p. However, it is unlikely that N_p is constant throughout the flame. Thus, if effects from N_p were dominant, one might expect a gradual, but noticeable change in $f_{v,blue} - f_{v,green}$ spatially at the 900 K case as the aggregates vary in size. Similarly, using a larger d_p results in higher $k_{e,blue}/k_{e,green}$ ratios at a given N_p from the RDG calculations. A similar argument as above can be used to rule out dominant effects from changing d_p.

Certainly the refractive index, m, plays an important role in the wavelength dependent differences observed in our evaluated f_v. Increasing only the imaginary part of m, which is the absorption component, leads to larger k_e values. Thus, the results at the 900 K ambient condition may indicate that absorption of blue light is more significant for the type of soot produced in this flame. Moving on to the 1200 K ambient condition shown in the lower panel of Figure 7, we observe spatial variation in $f_{v,blue} - f_{v,green}$. The larger soot volume fraction corresponding to the blue incident light data nearer to the injector and for the green incident light data farther away from the injector is an indication of the soot maturation process. As discussed in Shaddix et al. (Shaddix, Palotás et al. 2005), spectrally resolved extinction measurements in sooting premixed flames performed by Millikan (Millikan 1962), Bonne and Wagner (Bonne and Wagner 1965), and D'Alessio et al.(D'Alessio et al. 1972) showed that the dispersion coefficient decreased with increasing height above the burner. The dispersion coefficient provides a measure of how much m varies with wavelength. Soot having a higher dispersion coefficient was found to have a higher molar hydrogen-to-carbon (H/C) ratio. Soot precursor particles have been characterized by H/C ratios as high as 0.6, while the H/C ratio for carbonaceous soot is typically less than 0.2 (Shaddix, Palotás et al. 2005). In the 900 K conditions of Figure 7, $f_{v,blue} - f_{v,green}$ does not change significantly in space suggesting that the soot particle's optical properties are relatively constant. In the 1200 K conditions of Figure 7, an abrupt transition occurs in the quantity $f_{v,blue} - f_{v,green}$ near 30 mm. Based on the previous works discussed above, this transition is likely associated with a rapid decrease in the particles' H/C ratio as they transition from nascent to mature soot. Nevertheless, if multiple internal scattering by the agglomerates in these spray flames is significant, phenomena may be present that are not captured under the RDG approximation. Follow-on work will attempt to address these issues in more detail.

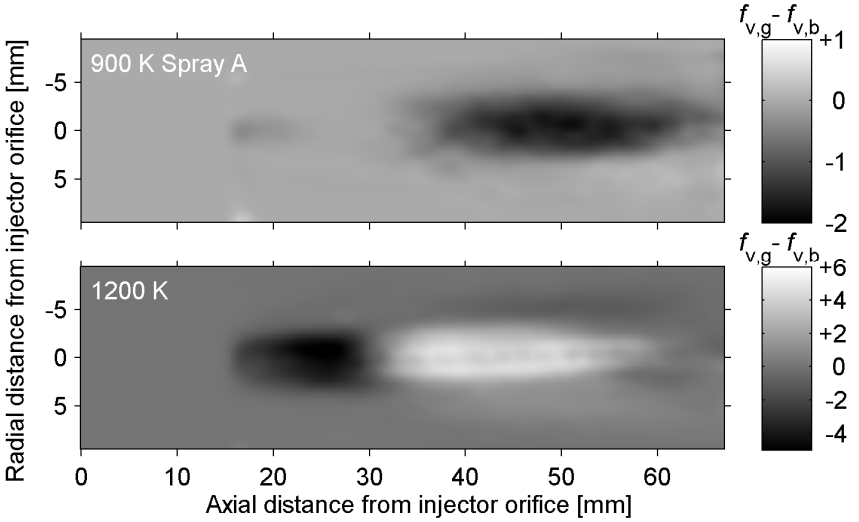

Figure 7. Difference between f_v corresponding to green LED extinction and f_v corresponding to blue LED extinction. The top and bottom panels correspond to the 900 K (Spray A) and 1200 K conditions, respectively.

3.2.3 Ambient temperature, density, and O_2 concentration effects on total soot mass

The mass of soot within 0.1-mm radial cross-sections along the flame axis is plotted in Figure 8 for the 850-1200 K ambient temperature conditions at an ambient density of 22.8 kg/m^3 and an ambient O_2 concentration of 15% by volume. The blue

curves correspond to mass computed from $f_{v,blue}$. The green curves correspond to soot mass computed from $f_{v,green}$. The total mass was calculated from f_v using an assumed density of 1.8 g/cm^3 for soot. Based on the results presented in Figure 7, the constant soot density assumption may introduce significant error for the higher ambient temperature cases. Nevertheless, since the soot density was held constant, the computed soot mass is proportional to f_v. In Figure 8, we see an increase in the length of the region where $f_{v,blue}$ is greater than $f_{v,green}$ at 1100 K when compared to the 1200 K case. This means that the region containing less-ordered soot is stretched out in physical space as the ambient temperature is reduced. The reverse is obviously true as ambient temperature increases. That is, we see more ordered soot earlier in the flame at higher ambient temperatures. At ambient temperatures of 1000 K and below, the data indicate that most of the soot formed in the flame absorbs stronger in the blue than in the green. We also point out that at axial positions near 60 mm and beyond, the mass of soot contained in the radial cross-sections for the 1000 K, 1100 K, and 1200 K cases is nearly the same. As discussed in Pickett and Siebers (Pickett and Siebers 2004), higher ambient temperatures lead to shorter lift-off lengths and larger equivalence ratios at *H*. Consequently, the soot mass peaks at an axial position closer to the injector, soot consumption (oxidation) begins at an earlier axial location, and soot oxidation kinetics are accelerated under higher ambient temperature conditions.

In Figure 9, we plot the inverse of the measured lift-off lengths along with the total soot mass in micrograms as a function of ambient temperature. The total soot mass is shown by the filled area, while the inverse lift-off lengths are represented by the curves. Ambient densities and oxygen concentrations in the left and right panels are distinguished by the different line styles. We observe that the inverse lift-off length is nearly linear with temperature for all ambient densities and oxygen concentrations. In the left panel, we find that the 13%, 15%, and 21% O_2 cases yield nearly the same total amount of soot at 900 K, while the 13% and 15% cases remain similar at 1000 K as well. Although the total soot data are similar at these temperatures, at 13% and 15% O_2 significant soot persists beyond the field of view. Thus, our integration does not include all soot formed in these flames. Since the 13% O_2 flame is lifted slightly more than the 15% O_2 flame, one might expect more soot outside our field of view in the former case leading to a larger total amount of soot (Idicheria and Pickett 2005). Of all cases studied, the 13% O_2, 22.8 kg/m^3, 1200 K case produces the largest amount of soot within our experimental field of view. In practice, this case represents conditions with high temperature, pressure, and exhaust gas recirculation (EGR). At ambient temperatures above 900 K, the 21% O_2 case forms about half the total amount of soot as the others. Although the higher O_2 concentration reduces soot due to the higher rate of oxidation, studies have shown that higher O_2 (and the resultant higher diffusion flame temperature) can also lead to significant amounts of nitrogen oxides (Plee et al. 1981; Ahmad and Plee 1983; Dec 1998).

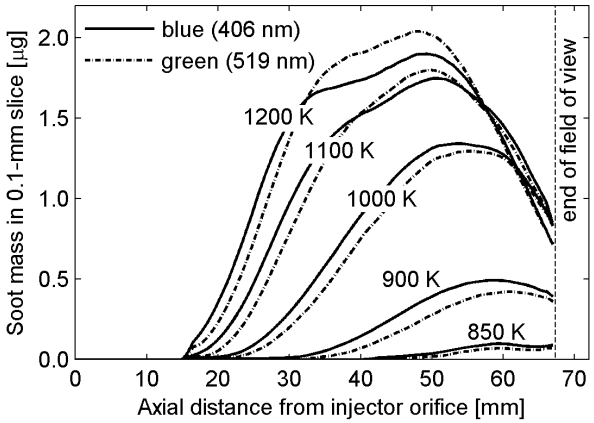

Figure 8. Soot mass in thin (0.1 mm) radial cross-sections of the jet as a function of axial distance from the injector orifice. Ambient density and O_2 concentration were 22.8 kg/m^3 and 15% by volume, respectively.

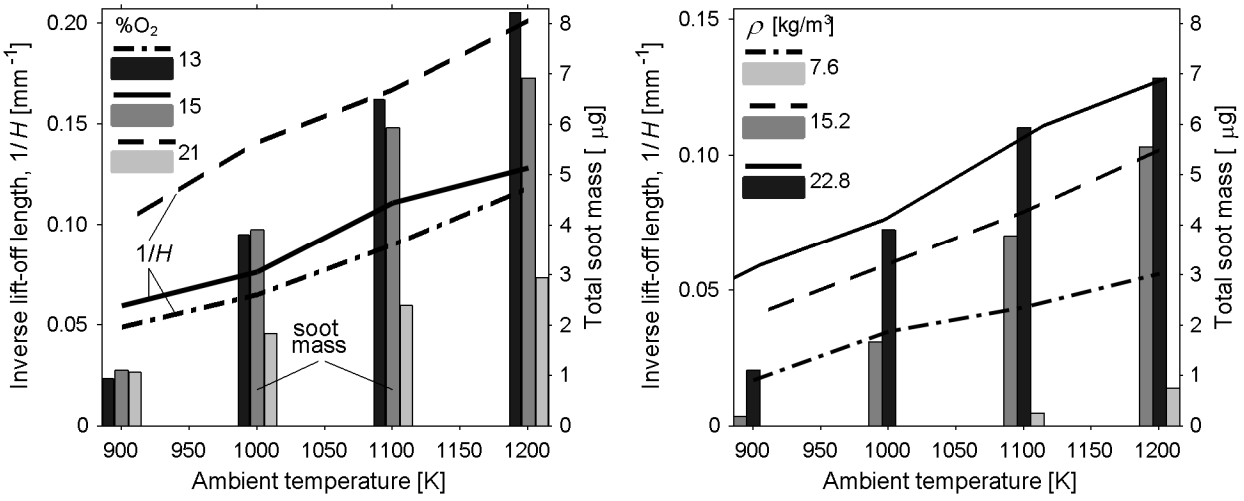

Figure 9. Inverse lift-off length, $1/H$ (curves) and total soot mass (filled area) as a function of ambient temperature.

The data in the right panel of Figure 9 show that the total soot mass increases significantly with increasing ambient density. As noted above, our field of view does not include the entire chamber. Consequently, the total soot mass evaluated for the three different density cases may be artificially low; however, this effect gets progressively worse as density is reduced and soot formation begins farther downstream. An interesting comparison can be made between the 13% O_2, ρ = 22.8 kg/m^3 data in the left panel and the 15% O_2, ρ = 15.2 kg/m^3 data in the right panel. Both cases are characterized by similar lift-off lengths as a function of ambient temperature; however, the 13% O_2, ρ = 22.8 kg/m^3 case yields between 40% and 100% more total soot mass depending on the ambient temperature. Though not shown here, a comparison of the axial soot mass profile for these two cases indicates that the onset of soot begins at an earlier axial location for the 13% O_2, 22.8 kg/m^3 case. Thus, the distance between the lift-off length and the onset of soot is reduced at the higher density. At least two factors driver greater soot production at higher ambient densities. First, higher densities promote more rapid soot formation kinetics since collisions occur more frequently, and second, higher ambient densities result in more fuel-rich mixtures at the lift-off length (Pickett and Siebers 2004). These results are consistent with prior work showing that the ambient oxygen concentration corresponding to the maximum soot yield decreases with increasing ambient density (Musculus and Pickett 2010).

4. Conclusions

In this work, we measured the lift-off length, ignition delay time, and soot volume fraction in n-dodecane spray flames under diesel engine relevant conditions. Lift-off lengths were measured by imaging OH chemiluminescence with an intensified camera during the quasi-steady period of the combustion event. Ignition delay times were measured based on the flame luminosity at wavelengths lower than 600 nm as acquired by a high-speed camera. Both the lift-off lengths and ignition delay times measured in this study under the "Spray A" condition (see www.sandia.gov/ECN) compared well with previous results obtained using the same combustion vessel, but a different fuel injector (with identical specifications). Agreement between the current and previous results is important as it confirms that the desired target thermodynamic conditions at injection were achieved.

Soot volume fraction was measured using a newly developed high-speed, 2-D, two-color extinction technique. The extinction setup uses high intensity, ultra-short pulse LEDs in conjunction with engineered diffusers and a field lens to produce pulsed, highly efficient diffused back-illumination. The diffused incident light greatly reduces the effects of beam steering, such that over the quasi-steady period of injection, the observed extinction due to beam steering is near zero. A relatively small amount of extinction attributed to beam steering was observed when viewing the individual time-resolved images, which defined the lower sensitivity limit of this technique for detecting soot volume fraction (~ 1 ppm). The measurements varying ambient density, temperature and oxygen concentration showed good agreement with previous works using laser extinction and/or LII measurements. We observed distinct differences between the soot volume fractions determined using the two different wavelengths of incident light. The blue light (406 nm) showed sensitivity toward the detection of younger soot particles characterized by less-order or lower elemental-to-total carbon ratios. The green light (519 nm) showed sensitivity toward the detection of more mature soot particles characterized by greater internal order and higher elemental-to-total carbon ratios.

The largest amount of total soot mass was observed under high-temperature, high-density, and low oxygen concentration conditions. These results indicate that the use of too much EGR at high temperature and pressure in diesel engines can lead to copious amounts of soot.

Acknowledgements

The authors wish to thank Chris Carlen (Sandia National Laboratories) for his efforts in the design and manufacturing of specific ultra-fast LEDs and David Cicone (Sandia National Laboratories) for technical support. The research was performed at the Combustion Research Facility, Sandia National Laboratories, Livermore, California. Sandia is a multiprogram laboratory operated by Sandia Corporation, a Lockheed Martin Company, for the United States Department of Energy's National Nuclear Security Administration under contract DE-AC04-94AL85000.

References

Ahmad, T.and S. L. Plee (1983). "Application of flame temperature correlations to emissions from a direct-injection diesel engine." SAE 831734.

Aizawa, T., H. Nishigai, K. Kondo, et al. (2012). "Transmission Electron Microscopy of Soot Particles Directly Sampled in Diesel Spray Flame - A Comparison between US#2 and Biodiesel Soot." SAE Int. J. Fuels Lubr. **5**(2): 665-673.

Bonne, U.and H. G. Wagner (1965). "Untersuchung des reaktionsablaufs in fetten kohlenwasserstroff-sauerstoff-flammen 3. Optissche untersuchungen an russenden flammen." Ber. Bunsenges. Physik Chem **69**: 35.

D'Alessio, A., F. Berettaand C. Venitozzi (1972). "Optical Investigations on Soot Forming Methane-Oxygen Flames." Combustion Science and Technology **5**(1): 263-272.

Dec, J. E. (1998). "PLIF Imaging of NO formation in a DI diesel engine." SAE 980147.

Ghandhi, J. B.and D. M. Heim (2009). "An optimized optical system for backlit imaging." Review of Scientific Instruments **80**(5).

Higgins, B.and D. Siebers (2001). Measurement of the Flame Lift-Off Location on DI Diesel Sprays Using OH Chemiluminescence, SAE International.

Idicheria, C. A.and L. M. Pickett (2005). Soot Formation in Diesel Combustion under High-EGR Conditions, SAE International.

Kastengren, A. L., F. Z. Tilocco, C. F. Powell, et al. (2013). "Engine Combustion Network (ECN): Measurements of Nozzle Diameter and Hydraulic Behavior." Atomization and Sprays.

Kook, S.and L. M. Pickett (2012). "Soot Volume Fraction and Morphology of Conventional, Fischer-Tropsch, Coal-Derived, and Surrogate Fuel at Diesel Conditions." SAE Int. J. Fuels Lubr. **5**(2): 647-664.

Koylu, U. O.and G. M. Faeth (1994). "Optical properties of overfire soot in buoyant turbulent diffusion flames at long residence times." Journal of Heat Transfer-Transactions of the ASME **116**(1): 152-159.

Koylu, U. O.and G. M. Faeth (1994). "Optical properties of soot in buoyant laminar diffusion flames." Journal of Heat Transfer-Transactions of the ASME **116**(4): 971-979.

Millikan, R. C. (1962). Sizes, optical properties, and temperatures of soot particles. Temperature: Its measurement and control in science and industry. New York, Reinhold Publishing. **3:** 497-507.

Musculus, M. P. B.and L. M. Pickett (2010). In-cylinder spray, mixing, combustion, and pollutant-formation processes in conventional and low-temperature combustion diesel engines. Advanced direct injeciton combustion engine technologies development. Volume 2: Diesel engines. H. Zhao. Cambridge, UK, Woodhead Publishing Limited**:** 644-675.

O'Connor, J.and M. Musculus (2013). "Post Injections for Soot Reduction in Diesel Engines: A Review of Current Understanding." SAE Technical Paper 2013-01-0917.

Pickett, L. M.and D. L. Siebers (2004). "Soot in diesel fuel jets: effects of ambient temperature, ambient density, and injection pressure." Combustion and Flame **138**(1-2): 114-135.

Pickett, L. M.and D. L. Siebers (2006). "Soot Formation in Diesel Fuel Jets Near the Lift-Off Length." International Journal of Engine Research **7**(2): 103-130.

Plee, J. T., J. P. Myersand T. Ahmad (1981). "Flame temperature correlation for the effects of exhaust gas recirculation on diesel particulate and NOx emissions." SAE 811195.

Puri, R., T. F. Richardson, R. J. Santoroand R. A. Dobbins (1993). "Aerosol dynamic processes of soot aggregates in a laminar ethene diffusion flame." Combustion and Flame **92**(3): 320-333.

Schulz, C., B. F. Kock, M. Hofmann, et al. (2006). "Laser-induced incandescence: recent trends and current questions." Applied Physics B **83**(3): 333-354.

Shaddix, C. R., Á. B. Palotás, C. M. Megaridis, et al. (2005). "Soot graphitic order in laminar diffusion flames and a large-scale JP-8 pool fire." International Journal of Heat and Mass Transfer **48**(17): 3604-3614.

Siebers, D.and B. Higgins (2001). Flame Lift-Off on Direct-Injection Diesel Sprays Under Quiescent Conditions, SAE International.

Siebers, D. L. (1998). Liquid-Phase Fuel Penetration in Diesel Sprays, SAE International.

Sjöholm, J., R. Wellander, H. Bladh, et al. (2011). "Challenges for In-Cylinder High-Speed Two-Dimensional Laser-Induced Incandescence Measurements of Soot." SAE Int. J. Engines **4**(1): 1607-1622.

Sorensen, C. M. (2001). "Light scattering by fractal aggregates: A review." Aerosol Science and Technology **35**(2): 648-687.

Williams, T. C., C. R. Shaddix, K. A. Jensenand J. M. Suo-Anttila (2007). "Measurement of the dimensionless extinction coefficient of soot within laminar diffusion flames." International Journal of Heat and Mass Transfer **50**(7-8): 1616-1630.